SCIENTIFIC REPORTS

OPEN

Large anomalous Nernst effect in a skyrmion crystal

Yo Pierre Mizuta[1] & Fumiyuki Ishii[2]

Received: 10 February 2016
Accepted: 26 May 2016
Published: 16 June 2016

Thermoelectric properties of a model skyrmion crystal were theoretically investigated, and it was found that its large anomalous Hall conductivity, corresponding to large Chern numbers induced by its peculiar spin structure leads to a large transverse thermoelectric voltage through the anomalous Nernst effect. This implies the possibility of finding good thermoelectric materials among skyrmion systems, and thus motivates our quests for them by means of the first-principles calculations as were employed in this study.

Thermoelectric (TE) generation, harvesting waste heat and turning it into electricity, should play an important role in realizing more energy-efficient society and overcoming the global warming. Nevertheless, it is yet to be widely used, mainly due to its still limited efficiency. There have been many studies pursuing highly efficient TE systems with a large value of figure of merit: $Z_X = \sigma X^2/\kappa$, where σ and κ are longitudinal electrical and thermal conductivity respectively, and $X = S$ or N is the Seebeck or Nernst coefficient depending on whether we use the longitudinal or transverse voltage for power generation. Here we omitted labels xx or yy in σ and κ by assuming an isotropic system. Among those, our study sheds light on the anomalous effect of electrical conduction perpendicular to an electric field (anomalous Hall effect, AHE)[1] or to a temperature gradient (anomalous Nernst effect, ANE)[2] on TE performance, focusing on a particular contribution to the conductivity of AHE (ANE), namely the so-called *intrinsic* term $\sigma_{xy}^{\mathrm{int}}$ ($\alpha_{xy}^{\mathrm{int}}$) expressed as a functional of Berry curvature[3] $\Omega(\mathbf{k}) \equiv i\langle\partial_{\mathbf{k}}u|\times|\partial_{\mathbf{k}}u\rangle$ in momentum ($\mathbf{k}$) space as in the second formula of Eq. (2), where $|u_{\mathbf{k}}\rangle$ is the periodic part of a Bloch state.

Systems hosting AHE/ANE are found in magnetic materials, both normal semiconductors[4] and topological insulators[5]. We previously studied simple models of 2D electron gas in an interface composed of those materials[6,7]. The anomalous effect on Seebeck coefficient was fairly large there, but remained rather small compared to what will be reported in this paper, which can mainly be attributed to the limited magnitude of the anomalous Hall conductivity (AHC) $\sigma_{xy}^{\mathrm{int}} \leq 1$ there [The unit is taken to be e^2/h (with e and h being the electron charge and the Plank's constant respectively) for the AHC in 2D in this paper].

There have been several ideas proposed for obtaining large AHC, such as the manipulation of massive Dirac cones (each of them being the source of $\sigma_{xy}^{\mathrm{int}} = 1$) by controlling parameters[8], or the extension of system dimension in the normal-to-plane direction (2D to 3D)[9].

What we focus here is another one, namely, the control of real-space spin textures which are well known to induce another contribution to the AHE/ANE, often called the *topological* Hall/Nernst conductivity[10] σ_{xy}^{T} (α_{xy}^{T}) that also has a geometrical meaning related to $\sigma_{xy}^{\mathrm{int}}$ ($\alpha_{xy}^{\mathrm{int}}$). In terms of Berry-phase theory[3], the emergence of *topological* terms in the continuum limit (spin variation scale $\gg$ atomic spacing), is an analogue of the ordinary Hall effect with the external B field just replaced by *spin magnetic field* B_{spin}, which is the real-space Berry curvature $\Omega(\mathbf{R})$ itself, proportional to a quantity called *spin scalar chirality* $\chi_{ijk} \equiv \mathbf{m}_i \cdot \mathbf{m}_j \times \mathbf{m}_k$ reflecting the geometrical structure spanned by each spin trio ($\mathbf{m}_i$, $\mathbf{m}_j$, $\mathbf{m}_k$). Although it should be better to treat $\sigma_{xy}^{\mathrm{int}}$ and σ_{xy}^{T} on an equal footing, we will omit the latter (*topological*) term in the main part of this paper because the validity of the simple relation $B_{\mathrm{spin}} \propto \Omega(\mathbf{R})$ is not clear for our system of rather short spin variation scale. Still, the omission can be justified within this approximation (see Part A of Supplemental Information for details).

Among many possible spin textures, what we target here is the so-called skyrmion crystal (SkX) phase observed even near room-temperature[11], where skyrmions, particle-like spin whirls, align on a lattice. The skyrmion, originally discussed in nuclear physics, has been studied extensively these days in condensed matter physics as well. Typical SkX-hosting materials are some of the transition metal silicides/germanides: MnSi[12], MnGe[13], FeGe[11], or heterostructures such as monolayer Fe on Ir(111)[14], in all of which the Dzyaloshinskii-Moriya term,

[1]Graduate School of Natural Science and Technology, Kanazawa University, Kanazawa, 920-1192 Japan. [2]Faculty of Mathematics and Physics, Kanazawa University, Kanazawa, 920-1192 Japan. Correspondence and requests for materials should be addressed to Y.P.M. (email: mizuta@cphys.s.kanazawa-u.ac.jp) or F.I. (email: ishii@cphys.s.kanazawa-u.ac.jp)

a spin-orbit coupling effect peculiar to their inversion-asymmetric crystal structure, plays a crucial role in the emergence of skyrmions.

Regarding the AHE in skyrmionic systems, quantum AHE (QAHE), i.e. the AHE with a quantized AHC $\sigma_{xy}^{\rm int} = \sum_n C_n(e^2/h)$ with an integer C_n called Chern number of n-th band, has recently been predicted in some SkX models where the conduction electron spins are exchange-coupled to the SkX either strongly[15] or weakly[16], preceded by a report of QAHE in a meron (half-skyrmion) crystal[17]. In this paper we focus on the case Hamamoto *et al.* picked out[15], because of its particularly large $\sigma_{xy}^{\rm int}$ implying the possibility of large ANE as well, thanks to the close relation between AHE and ANE[2,18], and that is the main point we confirmed in this study.

At the end of this section, we stress that the computational method used in our study is based on first-principles, which can be applied to the exploration of realistic materials of SkX etc. from the same perspective.

Expressions of thermoelectric quantities

The formulae for the thermoelectric coefficients to be evaluated follow from the linear response relation of charge current: $\mathbf{j} = \tilde{\sigma}\mathbf{E} + \tilde{\alpha}(-\nabla T)$, where $\mathbf{E}$ and ∇T are the electric field and temperature gradient present in the sample.

Using the conductivity tensors $\tilde{\sigma} = [\sigma_{ij}]$ and $\tilde{\alpha} = [\alpha_{ij}]$, we obtain

$$\begin{cases} S & \equiv & S_{xx} \equiv \dfrac{E_x}{(\nabla T)_x} = \dfrac{S_0 + \theta_H N_0}{1 + \theta_H^2} \\ N & \equiv & S_{xy} \equiv \dfrac{E_x}{(\nabla T)_y} = \dfrac{N_0 - \theta_H S_0}{1 + \theta_H^2} = -S_{yx}. \end{cases} \tag{1}$$

Here we defined $S_0 \equiv \alpha_{xx}/\sigma_{xx}$, $\theta_H \equiv \sigma_{xy}/\sigma_{xx}$, $N_0 \equiv \alpha_{xy}/\sigma_{xx}$ for a simpler notation. The conductivities are expressed as[19–21] $\sigma_{ij} = e^2\mathcal{L}_{ij}^{(0)}$, $\alpha_{ij} = \frac{e\mathcal{L}_{ij}^{(1)}}{T}$, with $\mathcal{L}_{ij}^{(n)}$ defined as $\mathcal{L}_{ij}^{(n)}(\mu, T) = \int d\varepsilon \Sigma_{ij}(\varepsilon)(\varepsilon - \mu)^n \left(-\frac{\partial f}{\partial \varepsilon}\right)$, which in turn is a functional of the function $\Sigma_{ij}(\varepsilon)$ explicitly showing the energy dependence proper to the considered system, which is written as,

$$\Sigma_{xx}(\varepsilon) = \sum_{n,\mathbf{k}} \tau_{n\mathbf{k}} [\mathbf{v}_{n\mathbf{k}}]_x^2 \, \delta(\varepsilon - \varepsilon_{n\mathbf{k}}), \quad \Sigma_{xy}(\varepsilon) = \sum_{n,\mathbf{k}} [\Omega_{n\mathbf{k}}]_z \, \Theta(\varepsilon - \varepsilon_{n\mathbf{k}}) \tag{2}$$

In the above formulae, $e(<0)$, $\tau_{n\mathbf{k}}$, $f(\varepsilon, \mu)$, $\mathbf{v}_{n\mathbf{k}}$, $\varepsilon_{n\mathbf{k}}$, $\Omega_{n\mathbf{k}}$, μ, and Θ stand for the electron's charge, relaxation time (hereafter assumed to take a constant value τ), the Fermi-Dirac distribution function, (velocity, energy and $\mathbf{k}$-space Berry curvature) of an electron with wave number $\mathbf{k}$, chemical potential and Heaviside step function, respectively. The subscript index n is put on each band-resolved quantity.

Throughout this paper, since our 2D system has no periodicity in z direction, we discuss $\sigma_{ij} \equiv \sigma_{ij}^{2D} \equiv d \times \sigma_{ij}^{3D}$, which is independent of the film thickness d and has the dimension of e^2/h whose unit can be $(\mathrm{Ohm})^{-1}$, instead of *real* conductivity σ_{ij}^{3D}.

Note that the conventionally-discussed Seebeck coefficient S_0 estimated without considering Berry curvature is obtained by setting $\theta_H = 0$ and $N_0 = 0$ in Eq. (1).

See Part B of Supplemental Information for some mathematical expressions needed to obtain the above expressions.

Model

We consider a magnetic SkX on a two dimensional square lattice, with its unit cell of lattice constant $2\lambda = 1.98$ nm containing 6×6 spins, thus the atomic lattice spacing $a = 2\lambda/6$ being 3.3 Å. This size of 2λ roughly corresponds to the smallest 3 nm as observed in MnGe[13] (We studied larger ones as well, and the obtained size-dependence is shown in Supplemental Information C). The spin configuration is equivalent to the one Hamamoto *et al.* studied[15], i.e., the spherical coordinates of spin $\mathbf{m}(\mathbf{r}_i)$ located at site i are set as $\theta_i = \pi(1 - r_i/\lambda)$ for $r_i < \lambda$ and $\theta_i = 0$ for $r_i > \lambda$, along with $\phi_i = \tan^{-1}(y_i/x_i) +$ (arbitrary constant). The spin modulation in the system is shown in Fig. 1. This fixing of spins corresponds to the strong limit of Hund's coupling to localized spins. In order to simulate the simplest case, we assume each spin is that of a hydrogen atom. We suppose our model, in the sense that it has a single orbital per site, is somewhat close to such e_g-orbital systems as $SrFeO_3$ films, where the emergence of SkX-like topological spin textures has been implied[22]. The model has several limitations, though, with regard to its coverage of experimental situations, which are described in Supplemental Information E.

Methods

Our calculations consist of three steps: With *OpenMX* code[23] (1) obtain the electronic Bloch states $\{|\Psi_{n\mathbf{k}}\rangle = e^{i\mathbf{k}\cdot\mathbf{r}}|u_{n\mathbf{k}}\rangle\}$ and corresponding eigenenergies $\{\varepsilon_{n\mathbf{k}}\}$ of the target SkX, and using a functionality[24] implemented in *OpenMX*, which is based on the formalism proposed by Marzari *et al.*[25] and Souza *et al.*[26], calculate their overlaps $\{M_{mn}^{\mathbf{k},\mathbf{b}} \equiv \langle u_{m\mathbf{k}}|u_{n\mathbf{k}+\mathbf{b}}\rangle\}$ between neighboring $\mathbf{k}$-points $\mathbf{k}$ and $\mathbf{k}+\mathbf{b}$ on a grid, and the projections $\{A_{mn}^{\mathbf{k}} \equiv \langle \Psi_{m\mathbf{k}}|g_n\rangle\}$ of a guessed set of localized orbitals $\{|g_n\rangle\}$ onto the Bloch states, and with *Wannier90* code[27] (2) construct maximally localized Wannier functions (MLWF) as particular linear combinations of $\{|g_n\rangle\}$ at each $\mathbf{k}$ point using the three sets of data passed from step(1): $\{\varepsilon_{n\mathbf{k}}\}$, $\{M_{mn}^{\mathbf{k},\mathbf{b}}\}$ and $\{A_{mn}^{\mathbf{k}}\}$, then finally (3) compute from the obtained MLWF all the necessary transport quantities $\{\sigma_{ij}, \alpha_{ij}\}$ [and finally Eq. (1)] expressed according to the Boltzmann semiclassical transport theory, where we adopted constant-relaxation-time approximation with a fixed value of $\tau = 0.1$ ps,

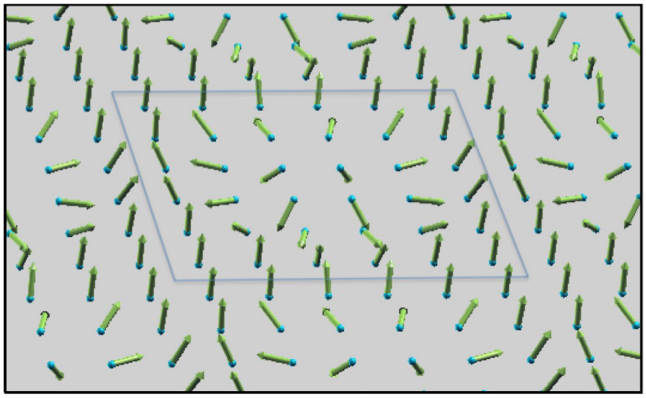

Figure 1. A view of an unit cell of 6 × 6 SkX.

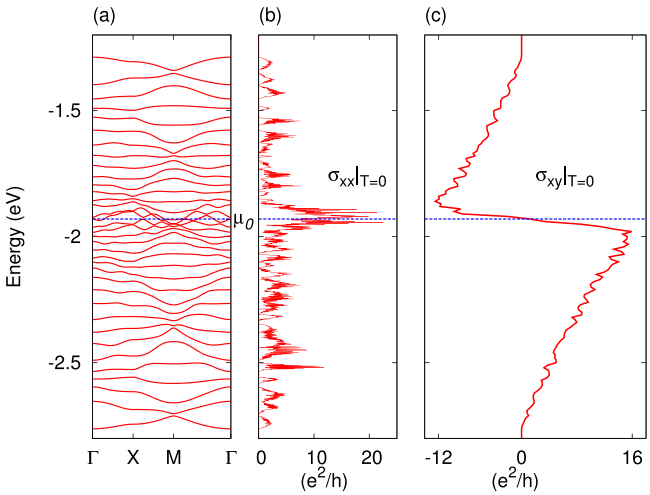

Figure 2. (**a**) Band structure and Fermi energy dependence of (**b**) longitudinal and (**c**) anomalous Hall conductivity of 6 × 6 SkX. The blue dashed line indicates the μ_0 mentioned in the main text.

a value expected to be realistic[28] (We will find, however, later in the discussions that our results are very sensitive to the choice of τ). In step(1), two *s*- and one *p*-character numerical pseudo-atomic orbitals with cutoff radius of 7 bohr was assigned to each H atom. The present calculation for a non-collinear magnetic system was realized by applying a spin-constraining method[29] in the non-collinear density functional theory[30]. Step(1) yielded $6 \times 6 = 36$ non-spin-degenerate occupied bands and the equal number of unoccupied ones, among which only the former 36 bands were used in step(2) to construct MLWF and interpolated with them to calculate the conductivities. In step(3), two modules were used in *Wannier90*: *berry* module based on the formalism proposed by Wang *et al.*[31] to compute $\Sigma_{xy}(\varepsilon)$ and *boltzwann* module introduced by Pizzi *et al.*[32] to compute σ_{xx} and S_0, in both of which the sampling for integrations was performed on 50×50 **k**-points. Besides these, numerical integrations were carried out to evaluate σ_{xy} and α_{xy} from $\Sigma_{xy}(\varepsilon)$.

The above procedure was tested in the following manner: For 4 × 4 SkX, the calculated band structure and the Fermi energy dependence of AHC were in overall agreement with the ones previously reported in the tight-binding model study[15], confirming the reproducibility of the similar situation by different approaches.

In addition, the AHC and the Berry curvature were computed also via another formalism, which is advantageous in the sense that it can identify the Chern number assigned to each band (see Supplemantal Information D), and the consistency was confirmed between the results from the two different methods.

Results and Discussions

Electronic structure and conductivities. First we show the obtained band structure of the 36 occupied states in Fig. 2(a). We notice there that each band is well isolated from each other, except for the four bands around the middle energy range $[-2.0, -1.9]$ eV, which we shall hereafter refer to as "central bands". Although we can hardly see gaps among the central bands on the scale of Fig. 2, we confirmed that even them are isolated from one another by finite gaps $\gtrapprox 10^{-2}$ meV (see Fig. 2 in Supplemental Information D). Another thing we notice is that some neighboring bands, including the central ones, tend to converge toward M point $(0.5, 0.5)\pi/(2\lambda)$. Regarding

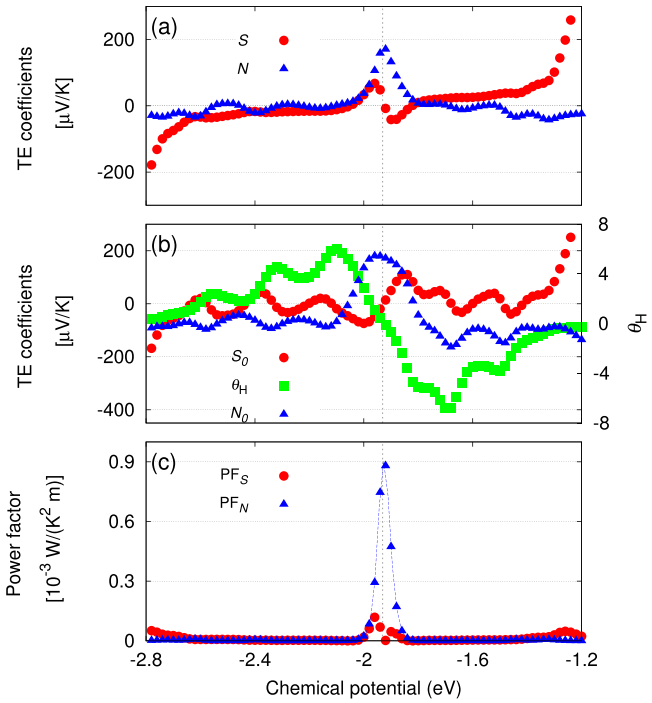

Figure 3. Chemical potential dependence of the thermoelectric quantities of 6×6 SkX at $T = 300$ K: (**a**) S and N, (**b**) S_0, N_0 (left axis) and θ_H (right axis) [see Eq. (1)], (**c**) Power factors corresponding to S and N. The blue dotted line for PF_N in (**c**) is drawn to guide the eye. The black dashed line indicates the μ_0 mentioned in the main text.

the dispersions, quite nice symmetry with respect to the energy $\mu_0 \simeq -1.93$ eV in the central bands also deserves close attention. Further analyses are needed in order to understand the secrets behind these interesting features.

Next, let us observe how the longitudinal conductivity σ_{xx} and AHC at $T = 0$ K, respectively equal to the function $e^2\Sigma_{xx}(\varepsilon)$ and $e^2\Sigma_{xy}(\varepsilon)$ in Eq. (2), depend on the band filling (Fermi energy) in Fig. 2(b,c) respectively. They are plotted in units of e^2/h, and thus the latter value is the occupied-states-sum of Chern numbers itself (in the sense generalized to non-integers in metallic situation). The $\sigma_{xx}(\mu)|_{T=0}$ has a large peak in the central bands region, as can be expected from the obviously large density of states there. The σ_{xx}'s roughly symmetric variation with respect to μ_0 (recognized when averaged over some broadened energy) could have been anticipated intuitively from the above-mentioned symmetric band structure.

The AHC, on the other hand, shows good anti-symmetric behavior with respect to μ_0, which is quite understandable from the combined consideration of, again, the symmetric band structure and the assumption that each of the well isolated (other than the central) bands is analogous to a Landau level formed by external magnetic field which contributes AHC $= 1$ (e^2/h) in the quantum Hall effect. The maximum absolute value of AHC is approximately 16, reached just below the central bands, while the second largest value of about 12 is located just above them (These maximums are smaller than the values 18 and 17 expected in an ideal case where no pair of bands overlaps at any energy, as is clear from Fig. 3 in Supplemental Information D). These behaviors result in the drastic change of AHC around the central bands as is prominent in Fig. 2(c). This very character has a strong effect on the TE properties of the system, as will be seen below.

Filling-dependence of thermoelectric properties. We will proceed to our main subjects, the TE quantities of the system, especially focusing on their electron filling dependence, which we assume to be parametrized by the chemical potential μ within the rigid band approximation. In all what is reported hereafter, the room temperature $T = 300$ K is assumed.

In Fig. 3, (a) Seebeck S and Nernst N coefficients, (b) S_0, θ_H, and N_0 [constituents of (a)], and (c) power factors associated with each of S and N, are shown, respectively.

As to the longitudinal $S(\mu)$, it is largely affected by the anomalous effect when $\theta_H(\mu)$ is finite (almost throughout the plotted μ range), except around the upper and lower edge, where $\theta_H \simeq 0$. We recognize in Fig. 3(a,b) the following two points (i) and (ii) including their explanation based on what we have seen in Fig. 2: (i) Just below and above μ_0, S shows the peaks (the higher one reaching $\approx 80\,\mu$V/K) of the sign opposite to that of S_0 despite rather small Hall angle θ_H there. This is thanks to the large N_0 that satisfies $|\theta_H N_0| > |S_0|$. (ii) Between the central and edge energy range, S is strongly suppressed compared to S_0 due to large θ_H.

On the transverse part N, what we notice in Fig. 3(a,b) and their interpretations are the following two points (i) and (ii): (i) Around μ_0, it shows a large peak $N \simeq N_0 \simeq 180\mu$V/K. This is because of $\theta_H(\mu_0) \simeq 0$ [see Eq. (1)] and large $\sigma'_{xy}(\mu_0)$ (the prime indicating the derivative with respect to μ at $T = 0$) as a result of the large

anti-symmetry of σ_{xy} around μ_0, which affects N_0 approximately through the Mott's relation [Eq. (3), later to be discussed quantitatively], which means $N_0 \propto \sigma'_{xy}/\sigma_{xx}$. (ii) Away from μ_0, N is strongly suppressed compared to N_0 due to large θ_H, similarly to the relation between S and S_0. This is different from the situation where N_0 is the far dominant contribution to N, as was previously reported[33].

In view of the relation between S and N, it is instructive that large N appears thanks to the large asymmetry of σ_{xy}, at the same filling where S diminishes due to the complete loss of asymmetry in σ_{xx}, showing that σ_{xy} could be an additional freedom in seeking better thermoelectricity, when the material is properly designed.

Before concluding this subsection, we comment on our choice $(a, T) = (3.3\,\text{Å}, 300\,\text{K})$: This is just an example of suitable sets for finding large N_0 in the following sense: If we obtain larger bandwidths, e.g. by compressing the lattice (making a smaller), while somehow keeping maximally the shape of Berry curvature, σ'_{xy} will be smaller, but thanks to the approximate relation $N_0 \propto \sigma'_{xy} T$ [see Eq. (3)], at a higher temperature we may well get N_0 of the same magnitude as in the original system.

Largest predicted thermoelectric voltages. In order to better capture quantitatively the above-mentioned connection between conductivities and TE coefficients that leads to large values of the latter, which are supposedly attractive for TE applications, let us check whether the largest values $S_{\max}$ and $N_{\max}$ seen in the central energy range in Fig. 3(a) can be roughly estimated via the well-known Mott's formula, which says,

$$\alpha_{ij} = -\frac{\pi^2}{3}\frac{k_B^2 T}{e}\sigma'_{ij}(\mu)\big|_{T=0}, \tag{3}$$

where k_B is the Boltzmann's constant. We write the chemical potential values that respectively give $S_{\max} > 0$ and $N_{\max} > 0$ as μ_S and μ_N, both of which are close to μ_0 but slightly different from one another ($\mu_N \simeq \mu_0 > \mu_S$). Finding that $S_0(\mu_S) \approx -40\,\mu\text{V/K}$, $\theta_H(\mu_S) \approx 1$, S reduces to $S(\mu_S) \simeq (-40 + N_0(\mu_S))/2 = -20 + \sigma'_{xy}/2\sigma_{xx}$. Similarly found is that $N(\mu_N) \simeq N_0(\mu_N)$ because of $S_0(\mu_N) \approx 0 \approx \theta_H(\mu_N)$. A rough estimation of $\sigma'_{xy}(\mu_S)|_{T=0}$ can be obtained by linearly-approximating the drastic drop of AHC $\Delta\sigma_{xy}(\mu) \approx -28(e^2/h)\Omega^{-1}$ in the energy range $\Delta\mu \approx 0.13\,\text{eV}$ in Fig. 2(c). This gives $\sigma'_{xy}(\mu_S) \simeq \frac{\Delta\sigma_{xy}}{\Delta\mu} \approx 2.2 \times 10^2 (e^2/h)\,\text{eV}^{-1}$. The other quantity we need is $\sigma_{xx}(\mu_S)$, which was found to be about $7.7(e^2/h)$. Combining these, a dimensionless factor of $x = k_B T/(\sigma_{xx}/\sigma'_{xy}) \simeq 0.73$ is found at $T = 300\,\text{K}$ ($k_B T \simeq 0.026\,\text{eV}$). Finally our evaluation arrives at $N_{\max} = N(\mu_N) \simeq N_0(\mu_N) \simeq N_0(\mu_S) \simeq -\frac{\pi^2}{3}\frac{k_B}{e}x \approx 2 \times 10^2\,\mu\text{V/K}$ and therefore $S_{\max} = S(\mu_S) \approx 1 \times 10^2 - 20 = 80\,\mu\text{V/K}$. These values are in fairly good accordance with the integration-derived values, hence clarifying that $T = 300\,\text{K}$ is *low* enough (in comparison to the Fermi level) for the Mott's formula to be valid at least for rough estimation.

At this point we compare the maximum value of $\alpha_{xy} \approx 10^{-8}\,\text{A/K}$ corresponding to the above-estimated $N_{\max}$, with a value presumably around the upper bound within low-T approximation for the two-band Dirac-Zeeman (DZ) model we studied before[7]. The low-T approximated α_{xy} in Eq. (4) of our previous study[7] can be rewritten as a 2D quantity $\alpha_{xy} \simeq (\pi k_B e/12h)(k_B T/\Delta)/\tilde{\mu}^2$, where Δ is the Zeeman gap and $\tilde{\mu} \equiv \mu/\Delta \geq 1$ for the electron-doped case. Assuming rather small $\tilde{\mu} = 2$, and choosing $(k_B T/\Delta) = 0.3$ to loosely satisfy the low-T criterion $k_B T \ll \mu - \Delta = \Delta$, we obtain $\alpha_{xy} \approx 10^{-10}\,\text{A/K}$ for the DZ model, which is by two orders of magnitude smaller than in the 6×6 SkX. Although some larger α_{xy} could be achieved beyond low-T range, still larger values in the SkX should be ascribed to the AHC more than ten times larger than that of the DZ model.

Finally, since $N_{\max} \simeq 180\mu\text{V/K}$ is a good enough value as a TE material, in order to further investigate the practical performance of the present system, we plot the power factor $\text{PF}_S \equiv \sigma_{xx} S^2$ and $\text{PF}_N \equiv \sigma_{xx} N^2$ in Fig. 3(c). Note that, for the evaluation of power factors, unlike in the discussions of TE quantities up to now, we need to know σ_{xx}^{3D}. Therefore we assumed the SkX film thickness of 10 nm. The maximum of $\text{PF}_N \approx 10^{-3}\,\text{W/(K}^2\text{m)}$ is comparable to the values of possible oxide TE candidates such as $NaCo_2O_4$ and ZnO[34]. Although the thermal conductivity κ was beyond the scope of this study, we just make a rough estimate here: Assuming the thermal conductivity κ of the order of 1 W/(Km) corresponding to good TE materials[34], the present case realizes $Z_N T$ of the order of 0.3 at $T = 300\,\text{K}$.

Please note, however, that the result is strongly dependent on the value of τ within our constant-τ approximation, as is clearly manifested in the relation $N(\mu_N) \propto \tau^{-1}$. For example we obtain $N(\mu_N) \approx 20\,\mu\text{V/K}$ if we suppose $\tau = 1$ ps, although the Nernst coefficient of this magnitude is still much larger than the so far reported values and is practically valuable[35].

Observing the striking properties of SkX phase, we believe it should be an important task to reveal the mystery behind it.

References

1. Nagaosa, N., Sinova, J., Onoda, S., MacDonald, A. H. & Ong, N. P. Anomalous Hall effect. *Rev. Mod. Phys.* **82,** 1539 (2010).
2. Xiao, D., Yao, Y., Fang, Z. & Niu, Q. Berry-phase effect in anomalous thermoelectric transport. *Phys. Rev. Lett.* **97,** 026603 (2006).
3. Xiao, D., Chang, M. C. & Niu, Q. Berry phase effects on electronic properties. *Rev. Mod. Phys.* **82,** 1959 (2010).
4. Culcer, D., MacDonald, A. & Niu, Q. Anomalous Hall effect in paramagnetic two-dimensional systems. *Phys. Rev. B* **68,** 045327 (2003).
5. Chang, C.-Z. *et al.* Experimental observation of the quantum anomalous Hall effect in a magnetic topological insulator. *Science* **340,** 167 (2013).
6. Mizuta, Y. P. & Ishii, F. Contribution of Berry curvature to thermoelectric effects. *JPS Conf. Proc.* **3,** 017035 (2014).
7. Mizuta, Y. P. & Ishii, F. Thermopower of doped quantum anomalous Hall insulators: The case of Dirac Hamiltonian. *JPS Conf. Proc.* **5,** 011023 (2015).
8. Fang, C., Gilbert, M. J. & Bernevig, B. A. Large-Chern-number quantum anomalous Hall effect in thin-film topological crystalline insulators. *Phys. Rev. Lett.* **112,** 046801 (2014).

9. Jiang, H., Qiao, Z., Liu, H. & Niu, Q. Quantum anomalous Hall effect with tunable Chern number in magnetic topological insulator film. *Phys. Rev. B* **85,** 045445 (2012).
10. Neubauer, A. *et al.* Topological Hall effect in the A phase of MnSi. *Phys. Rev. Lett.* **102,** 186602 (2009).
11. Yu, X. Z. *et al.* Near room-temperature formation of a skyrmion crystal in thin-films of the helimagnet FeGe. *Nature Mater.* **10,** 106 (2010).
12. Mühlbauer, S. *et al.* Skyrmion lattice in a chiral magnet. *Science* **323,** 915 (2009).
13. Kanazawa, N. *et al.* Large topological Hall effect in a short-period helimagnet MnGe. *Phys. Rev. Lett.* **106,** 156603 (2011).
14. Heinze, S. *et al.* Spontaneous atomic-scale magnetic skyrmion lattice in two dimensions. *Nature Phys.* **7,** 713 (2011).
15. Hamamoto, K., Ezawa, M. & Nagaosa, N. Quantized topological Hall effect in skyrmion crystal. *Phys. Rev. B* **92,** 115417 (2015).
16. Lado, J. L. & Fernández-Rossier, J. Quantum anomalous Hall effect in graphene coupled to skyrmions. *Phys. Rev. B* **92,** 115433 (2015).
17. McCormick, T. M. & Trivedi, N. Tuning the Chern number and Berry curvature with spin-orbit coupling and magnetic textures. *Phys. Rev. A* **91,** 063609 (2015).
18. Miyasato, T. *et al.* Crossover behavior of the anomalous Hall effect and anomalous Nernst effect in itinerant ferromagnets. *Phys. Rev. Lett.* **99,** 086602 (2007).
19. Allen, P. B., Pickett, W. E. & Krakauer, H. Anisotropic normal-state transport properties predicted and analyzed for high-T_c oxide superconductors *Phys. Rev. B* **37,** 7482 (1988).
20. Mahan, G. D. & Sofo, J. O. The best thermoelectric. *Proc. Natl. Acad. Sci. USA* **93,** 7436 (1996).
21. Hinsche, N. F. *et al. Ab-initio* description of the thermoelectric properties of heterostructures in the diffusive limit of transport. *Phys. Status Solidi A* **213,** 672 (2016).
22. Chakraverty, S. *et al.* Multiple helimagnetic phases and topological Hall effect in epitaxial thin films of pristine and Co-doped $SrFeO_3$. *Phys. Rev. B* **88,** 220405(R) (2013).
23. Ozaki, T. *et al. OpenMX*: Open source package for Material eXplorer. URL: www.openmx-square.org.
24. Weng, H., Ozaki, T. & Terakura, K. Revisiting magnetic coupling in transition-metal-benzene complexes with maximally localized Wannier functions. *Phys. Rev. B* **79,** 235118 (2009).
25. Marzari, N. & Vanderbilt, D. Maximally localized generalized Wannier functions for composite energy bands. *Phys. Rev. B* **56,** 12847 (1997).
26. Souza, I., Marzari, N. & Vanderbilt, D. Maximally localized Wannier functions for entangled energy bands. *Phys. Rev. B* **65,** 035109 (2001).
27. Mostofi, A. A. *et al. Wannier90*: A tool for obtaining maximally-localised Wannier functions. *Comput. Phys. Commun.* **185,** 2309 (2014).
28. Shur, M., Gelmont, B. & Asif Khan, M. Electron mobility in two-dimensional electron gas in AlGaN/GaN heterostructures and in bulk GaN. *J. Electron. Mater.* **25,** 777 (1996).
29. Kurz, Ph., Förster, F., Nordström, L., Bihlmayer, G. & Blügel, S. *Ab initio* treatment of noncollinear magnets with the full-potential linearized augmented plane wave method. *Phys. Rev. B* **69,** 024415 (2004).
30. Kübler, J., Höck, K-H., Sticht, J. & Williams, A. R. Density functional theory of non-collinear magnetism. *J. Phys. F.* **18,** 469 (1988).
31. Wang, X., Yates, J. R., Souza, I. & Vanderbilt, D. *Ab initio* calculation of the anomalous Hall conductivity by Wannier interpolation. *Phys. Rev. B* **74,** 195118 (2006).
32. Pizzi, G., Volja, D., Kozinsky, B., Fornari, M. & Marzari, N. *BoltzWann*: A code for the evaluation of thermoelectric and electronic transport properties with a maximally-localized Wannier functions basis. *Comput. Phys. Commun.* **185,** 422 (2014).
33. Hanasaki, N. *et al.* Anomalous Nernst effects in pyrochlore molybdates with spin chirality. *Phys. Rev. Lett.* **100,** 106601 (2008).
34. Gaultois, M. W. *et al.* Data-driven review of thermoelectric materials: Performance and resource considerations. *Chem. Mater.* **25,** 2911 (2013).
35. Sakuraba, Y. Potential of thermoelectric power generation using anomalous Nernst effect in magnetic materials. *Scr. Mater.* **111,** 29 (2016).

Acknowledgements

The authors thank K. Hamamoto for providing us with detailed information on the model he and coworkers had studied. We also thank N. Nagaosa for his insightful remarks, H. Sawahata and H. Weng for their discussions on the computation of Chern number. This work was partially supported by Grants-in-Aid on Scientific Research under Grant Nos 25790007, 25390008 and 15H01015 from Japan Society for the Promotion of Science and by the MEXT HPCI Strategic Program. This work was also supported by Kanazawa University SAKIGAKE Project. Computations in this research were performed using supercomputers at ISSP, University of Tokyo.

Author Contributions

Y.P.M. performed the numerical calculations, while F.I. implemented a code for computing Chern number. Y.P.M. and F.I. discussed the results and prepared the manuscript together. F.I. supervised this project. Correspondence and requests for materials should be addressed to Y.P.M. or F.I.

Additional Information

Supplementary information accompanies this paper at http://www.nature.com/srep

Competing financial interests: The authors declare no competing financial interests.

How to cite this article: Mizuta, Y. P. and Ishii, F. Large anomalous Nernst effect in a skyrmion crystal. *Sci. Rep.* **6**, 28076; doi: 10.1038/srep28076 (2016).